Local Structure Studies of As-Made Cu_2ZnSnS_4 Nanoparticles

Leila Jewell, Sophia Rocco, Frank Bridges,* and Sue A. Carter

Physics Department, University of California, Santa Cruz, California 95064, USA

(Received 18 January 2017; revised manuscript received 12 May 2017; published 26 June 2017)

Though Cu_2ZnSnS_4 (CZTS) is a promising material for thin-film solar cells, a significant challenge remains in understanding the structures being formed, particularly in nonstoichiometric materials. We use the extended x-ray absorption fine-structure technique to study the local structure and stoichiometry of as-made, Cu-deficient CZTS nanoparticles and present *K*-edge data and fits for each of the cations (Cu, Zn, and Sn). The data show that all of the metal-S (*M*-S) pairs have the bond lengths of the kesterite structure within 0.02 Å, and the pair distribution function is very narrow ($\sigma \sim 0.07$ Å). These results preclude significant fractions of other phases with different *M*-S bond lengths. The data also reveal some Sn second neighbors around Sn, whereas there are none in the stoichiometric kesterite (or stannite) structure. Consequently, Sn antisite defects must be present on Cu or Zn sites; this is not surprising since there is some excess of Sn. More importantly, the second-neighbor Sn-Sn distance is significantly longer than other *M*-*M* distances, and the antisite Sn defects must therefore introduce significant disorder within the Cu and Zn sublattices. The largest distortions are found around Cu and are modeled using a strongly broadened (or split) peak distribution for the Cu-Cu/Zn pairs. We also find that excess Zn does not occupy Cu sites but instead, goes onto Sn sites. The samples are best described as a kesterite structure with significant antisite disorder.

DOI: 10.1103/PhysRevApplied.7.064026

I. INTRODUCTION

Cu_2ZnSnS_4 (CZTS) has many desirable properties for solar-cell applications: low-cost, abundant materials, an optimal band gap, and promising initial solar-energy conversion efficiencies [1]. Some of the highest efficiency devices have been fabricated from solution-processible nanoparticles [2] as the starting material rather than bulk materials. The nanoparticles may form different structure and/or stoichiometry than bulk systems.

Controlling the stoichiometry and structure of CZTS has, in general, proved challenging [3,4]. The materials ZnS and Cu_2S are nearly immiscible [5], and SnS_2 is needed to stabilize the CZTS structure. Because the range of stability in the ZnS-Cu_2S-SnS_2 phase diagram is small [6], many samples made at low temperatures are not stoichiometric. The stoichiometry of nanoparticles can be tuned to have a band gap of 1.5 eV, which has applications in photovoltaics and light-emitting-diode lighting [7,8].

A major difficulty, however, is in characterizing the local structures that form within CZTS and related materials, around each of the cations. The local arrangement of atoms is very similar to a cubic zinc-blende structure such as cubic ZnS, with 4 S nearest neighbors and 12 metal second neighbors. The ordering of the metal atoms leads to the kesterite or stannite structure, with the primary difference arising from an interchange of the Zn and one of the Cu atom sites between the two structures [9].

The environments around each cation are consequently very similar, as seen in the crystal structure, shown in Fig. 1. In diffraction, the main Bragg peaks of CZTS are at nearly the same position as that of several related compounds and components, including Cu_2SnS_3 and ZnS, which makes it very difficult to distinguish such components. Additionally, the grain size in thin films can be small, leading to broader peaks, and for small nanoparticles, often only a few broad diffraction peaks remain. Other groups have synthesized CZTS materials in powder [10] and thin films [11], and some extended x-ray absorption fine-structure (EXAFS) studies have been carried out on these materials [12–17]; x-ray absorption near edge structure (XANES) studies at the S edge (and at the Se *K* edge for CZTSe) have also been carried out for thin-film samples [18,19], but there is little to compare directly with our data. However, we include these results in Sec. V.

Here, we study the local structure in as-made, slightly off-stoichiometry nanoparticles of CZTS to see how or if the structure differs from bulk materials. Here, the samples are Cu poor, as Guo *et al.* [2] note that such materials make better devices, while other phases form for Cu-rich samples. We use the EXAFS technique to determine the environment around Cu, Zn, and Sn, out to the third shell of neighbors. Some earlier EXAFS studies [12–14,16] have investigated the local structure in CZTS materials, but many are not in nanoparticle form; also, they have rather different results, which are compared in Sec. V. In addition, we use the absorption step height for each metal element to estimate atomic ratios, and hence the composition. This approach provides a direct measure of the stoichiometry of

*Corresponding author.
bridges@ucsc.edu

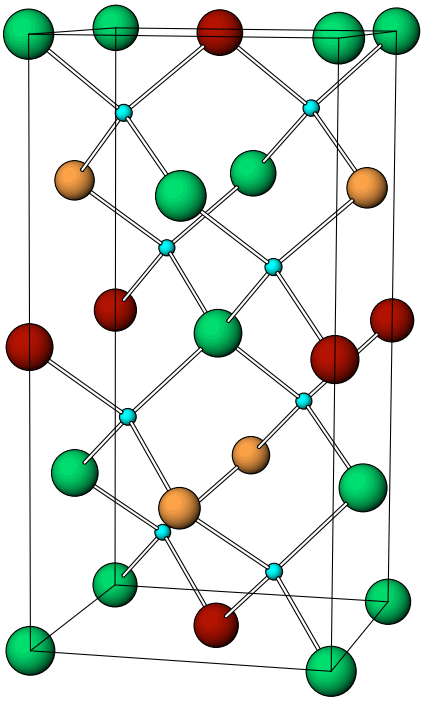

FIG. 1. The structure of kesterite Cu_2ZnSnS_4; the unit cell is tetragonal (space group $I\bar{4}$). The Cu atoms are green spheres, the Zn atoms are orange spheres, the Sn atoms are dark-red spheres, and the S atoms are small light-blue spheres. Other possible structures are stannite CZTS and zinc-blende CZTS. Stannite is nearly identical to kesterite, only the Zn sites switch locations with one of the two Cu sites. This change is indistinguishable to EXAFS since Cu/Zn are neighbors in the periodic table. A third possible CZTS structure is a distorted zinc-blende structure, which has a random distribution of metal atoms on the cation sites.

the sample under study, and the composition extracted from step heights agrees well with other methods such as energy-dispersive x ray [20] and atomic absorption [21].

Espinosa-Faller *et al.* [16] study the local structure of stoichiometric CZTS in nanoparticle form. Our two (different) nanoparticle samples are both slightly copper poor, which may produce better devices [1,2,4,22]. Owing to the Cu deficiencies, the two samples are also either zinc rich or tin rich, which provides some contrast. It is important to see if these shifts in the stoichiometry change the local structure of CZTS, such as whether significant clustering occurs or whether the cations have the approximate orderings required for the known kesterite and stannite structures. Additionally, because Cu_2SnS_3 and ZnS have very similar diffraction patterns, one needs to determine if phase separation occurs, i.e., whether significant fractions of these two (or other) compounds are also present. A complication for nanoparticle samples is that the diffraction peaks become significantly broadened and the difference between CZTS, Cu_2SnS_3, ZnS, and other similar phases cannot be resolved. Unfortunately, because Cu and Zn are neighbors in the periodic table, the EXAFS signals for Cu and Zn are nearly identical and one cannot distinguish between Cu and Zn neighbors.

II. EXPERIMENTAL DETAILS

A. Samples

For this study, two different nanoparticle materials (of approximately 7 nm diameter), were purchased from Mesolight, who synthesized them in June, 2014 [2,23]. We have diffraction data for these samples, but only three broad peaks are observed at the positions of the three dominant lines, and that is not useful for understanding the structure. For the EXAFS samples, the nanoparticles, suspended in toluene, are deposited into the filter paper by pipetting the solution onto the paper and then evaporating the solvent. Using multiple cycles of pipetting and evaporation, sufficient CZTS is deposited into the filter paper so that, with several layers of filter paper to adjust the step height for each edge, the x-ray absorption can be measured in transmission.

B. Data collection

The EXAFS data were collected at the Stanford Synchrotron Radiation Lightsource (SSRL) on beam lines 11-2 and 4-1 (unfocused mode) using a Si (220) double monochromator, detuned 30% for all edges to reduce harmonics. Slit heights were approximately 0.5 mm, which gives energy resolutions of about 0.9 eV for Cu and Zn and approximately 6.9 eV for Sn. The Cu, Zn, and Sn K-edge data were collected in transmission mode at a temperature of 50 K for sample 1 and 8 K for sample 2. A minimum of three scans was collected for each edge for averaging and to check reproducibility. Previous studies of bulk ZnS have shown very little change in the EXAFS data from 8 to 50 K [24,25], with no change in the first (Zn-S) peak and only a tiny change of a few percent in the second peak (Zn-Zn); thus, there was no significant temperature effect.

In addition, XANES data were collected at the same time for each edge. In each case, the data for the two samples overlapped very well. The only clear change is a tiny (1%) increase in the preedge peak near 8985 eV for the Cu K-edge XANES of sample 1, which has a larger Cu/Zn ratio than sample 2 does. By contrast, the recent work of Colina-Ruiz *et al.* [17] found that this peak decreased slightly for larger Cu/Zn ratios (but for larger Cu/Sn ratios). Thus, tiny changes in the Cu preedge peak do not provide a clear monitor of composition, and we do not consider the XANES further.

III. DATA

A. EXAFS data

The EXAFS data are reduced using standard procedures [26], which include removing the preedge background using the Victoreen equations [27] for transmission data and extracting the EXAFS oscillations, $\chi(E)$, with a spline fit of the postedge background. This function is converted

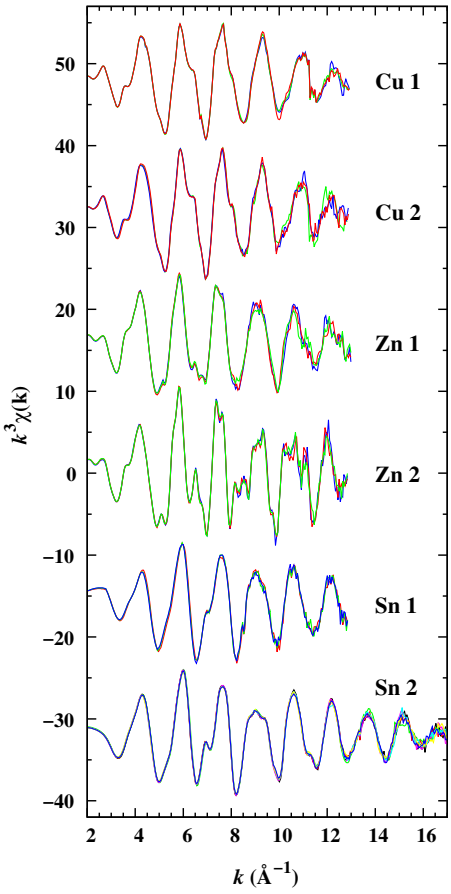

FIG. 2. k-space data $[k^3\chi(k)]$ for the Cu K, Zn K, and Sn K edges of two CZTS samples at $T = 50$ K (no. 1) and 8 K (no. 2). Three traces are plotted for each edge (seven traces for Sn 2) to show the reproducibility of the data. The largest difference between the samples is observed for the Zn K edge.

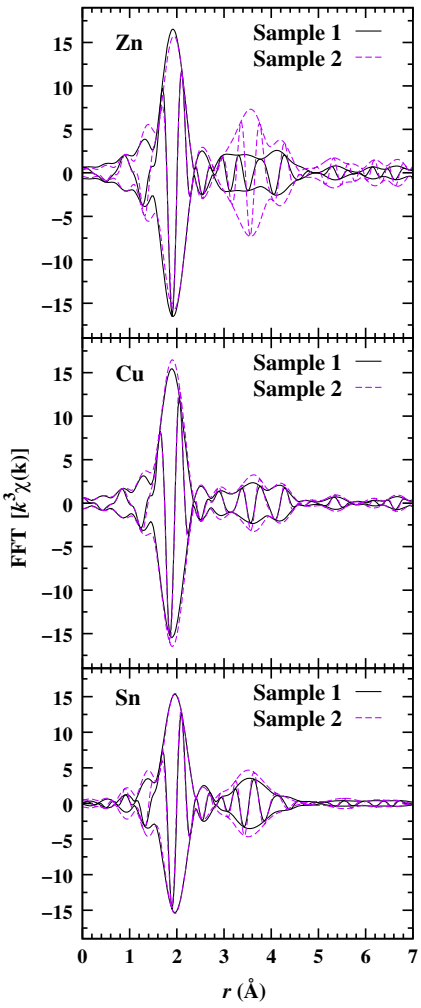

FIG. 3. EXAFS r-space data for the Zn, Cu, and Sn K edges of samples 1 and 2. The strong similarities in shape indicate that all of the elements are in a similar environment. The largest peak near 1.9 Å is the first S neighbor. Here and in the following r-space plots, the fast oscillation is the real part, R, of the FFT; the amplitude function is $\pm\sqrt{R^2 + I^2}$, where I is the imaginary part (not plotted) of the FFT. The FT window is 3.5–11.5 Å^{-1}, Gaussian broadened by 0.3 Å^{-1}.

to k space using the relation $k = \sqrt{[2m(E - E_0)]/\hbar^2}$, where E_0 is experimentally determined as the energy at the half height of the edge step. The k-space EXAFS data for each metal K edge are shown in Fig. 2, and they are highly reproducible with little variation between scans. Note that the Sn-edge data of sample 2 actually has seven data traces, which shows the high repeatability of the data. An average of these traces is used in the following data analysis and fits.

The k-space data are fast Fourier transformed (FFT) into r space using a FT range of 3.5–11.5 Å^{-1} (the FT window is Gaussian rounded by 0.3 Å^{-1}), as shown in Fig. 3 for a k^3 weighting—FFT$[k^3\chi(k)]$. Peaks in r space correspond to different shells of neighbors, but the peak positions are always shifted to lower r's compared to the actual pair distance—in this case, by approximately 0.4 Å for S neighbors. For well-ordered material, peaks exist well beyond 6 to 7 Å; generally, the larger the amplitudes of the further neighbor peaks are, the more ordered the compound is. For all three edges—but particularly for Zn—sample 2 has more well-defined peaks at high r, which means it is more ordered than sample 1.

B. Composition

The composition results for the two samples are shown in Table I. These results are determined from the absorption step height for each edge, measured at the same point on the same sample in a difference set of scans. Note that, for such measurements, the sample needs to be thin enough that the step height for the lowest energy edge is not too large (<1); otherwise, pinhole effects [28,29] distort the edge and make the observed step height too small. The step heights are converted to concentration ratios using the McMaster tables [30], following the approach we have used successfully in the

TABLE I. Ratios of metal cations and relative composition of the CZTS samples, assuming four S atoms. These ratios highlight the excess Sn and deficient Zn fractions in sample 1, and the excess Zn and deficient Cu in sample 2.

Ratios	No. 1	No. 2	Composition	No. 1	No. 2
Cu/Zn	2.37	1.47	Cu	1.89	1.75
Cu/Sn	1.45	1.64	Zn	0.80	1.19
Zn/Sn	0.61	1.12	Sn	1.31	1.06
Cu/(Zn + Sn)	0.90	0.77	S	(4)	(4)

TABLE II. Number of Cu/Zn and Sn neighbors around Cu, Zn, and Sn for samples 1 and 2, based on the distributions on each site described in the text: $[Cu][Cu_{0.89}Sn_{.11}][Zn_{0.8}Sn_{0.2}][Sn]$ and $[Cu][Cu_{.75}Sn_{.25}][Zn][Sn_{0.81}Zn_{0.19}]$.

	Sample 1		Sample 2	
Metal edge	*M*-Cu/Zn	*M*-Sn	*M*-Cu/Zn	*M*-Sn
Cu	7.0	5.0	8.2	3.8
Zn	7.6	4.4	8.3	3.7
Sn	10.0	2.0	10.5	1.5

past [20,21]. Sample 1 contains too much Sn in the sample, with some Zn deficiency as well. For four S atoms (the EXAFS results presented later confirm the fourfold S coordination of a kesterite structure for each metal atom), these ratios yield a composition of $Cu_{1.89}Zn_{0.80}Sn_{1.31}S_4$, shown in Table I. By contrast, sample 2 is instead Zn rich, with Sn close to stoichiometric, while still being Cu poor. The resulting composition is $Cu_{1.75}Zn_{1.19}Sn_{1.06}S_4$. Samples 1 and 2 provide a means for studying how varying Sn concentrations influence the distribution of the metal atoms.

The off-stoichiometric composition raises several questions: are other phases present and, if not, how are the Cu, Zn, and Sn arranged in the kesterite structure? From the later EXAFS analysis, we will argue that possible phases such as ZnS or Cu_2SnS_4, etc., are, at most, a few percent, and we therefore concentrate here on the kesterite structure, including possible antisite defects. Specifically for the 12 second-neighbor metal atoms, what is the atomic distribution around a given element? Because Cu and Zn are neighbors on the periodic table, such neighbors cannot be discriminated and only the numbers of Cu/Zn and Sn are considered. The kesterite structure has four distinct metal sites, *S*1–*S*4, occupied by Cu1, Cu2, Zn and Sn. An interesting feature of this structure is that no site has second neighbors of the same site—e.g., the metal neighbors on *S*1 have four atoms each on sites *S*2, *S*3, and *S*4. Thus, if a type of atom is on only one site (as is the case for Sn in stoichiometric CZTS), there will be no Sn neighbors around any Sn atoms. If the fractional occupancy on each site is known, one can easily calculate the number of Cu/Zn and Sn neighbors around Cu, Zn, or Sn. Based on earlier work that showed that CuS and ZnS do not mix [5], the occupation of each site is set by the following assumptions: (1) there is no exchange of Cu and Zn between their sites, and (2) excess Sn can go onto either Cu or Zn sites. For sample 1, excess Sn is placed on both the Cu and Zn site to give the following distribution on the four sites: $[Cu][Cu_{0.89}Sn_{.11}][Zn_{0.8}Sn_{0.2}][Sn]$. Sample 2 has excess Zn; in this case, the excess Zn is placed on the Sn site and some Sn is shifted to a Cu site to give: $[Cu][Cu_{.75}Sn_{.25}][Zn][Sn_{0.81}Zn_{0.19}]$. (Note that if the excess Zn were placed on Cu sites, then there would be very few Sn neighbors around Sn—in strong disagreement with the results discussed below.) From these distributions, the expected number of neighbors around Cu, Zn, and Sn are calculated and tabulated in Table II.

C. Local structure

The *r*-space data for the Cu, Zn, and Sn *K* edges look very similar in shape, as shown in Fig. 3. The large peak near 1.9 Å corresponds to the four S atoms in the first shell of neighbors around each metal atom (actual distances from diffraction of about 2.33–2.4 Å). The position of this peak is nearly the same for each edge, suggesting comparable metal-S bond lengths. This result is expected in CZTS, but not for individual sulfides such as CuS and Cu_2S (shorter Cu—S bonds) or SnS and SnS_2 (longer Sn—S bonds). The second shell peak, near 3.5 Å (an actual distance of about 3.8 Å), consists of 12 metal neighbors of Cu, Zn, or Sn for bulk material, but it might be somewhat less for very small nanoparticles, depending on size; e.g., for ZnS particles of approximately 3 nm, there are about nine or ten Zn second neighbors [24]. Note that the peak positions are nearly the same for all edges, as was also observed by Espinosa-Faller *et al.* [16]. By contrast, Bacewicz *et al.* [14] found the metal-metal peaks at a longer distance, while Siah *et al.* [12] found the first metal-S peaks at distances with even greater deviations from diffraction results, with negative shifts of 0.07–0.08 Å for Zn-S and positive shifts of 0.06–0.07 Å for Sn-S, though they report only Δr, without stating the starting pair distance.

Another unusual feature of our data comes from a comparison of the Cu and Zn *K*-edge data; because Cu and Zn are neighbors in the periodic table, the simulated EXAFS using FEFF8.5 [31] are essentially identical. Experimentally, however, the second-neighbor peak in the Zn-edge data is much larger than for the Cu-edge data, particularly for sample 2. A similar result was shown in *r*-space plots by Espinosa-Faller *et al.* [16]; the similarity might be related to the fact that both their study and ours use nanoparticle samples. However, as discussed below, it is more likely the distribution of atoms on the various sites.

Theoretical functions for each atom pair are generated using FEFF8 [31]. Note that the second-neighbor Cu and Zn backscatterers are nearly indistinguishable—i.e., the metal-Cu and metal-Zn functions are nearly the same. Consequently, in fits, a Cu second-neighbor pair function is used to represent both the Cu and Zn second neighbors.

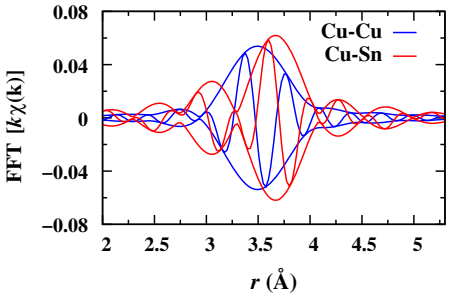

FIG. 4. A comparison of the theoretical r-space functions for Cu-Cu and Cu-Sn second-neighbor peaks (these functions correspond to one neighbor at the same distance and are not broadened). Note that the real part of the Fourier transform (fast oscillating function) for Cu-Cu is nearly 180° out of phase with that for Cu-Sn; consequently, a sum of these functions is significantly reduced, and the peak position may be shifted.

By contrast, the complex parts of the theoretical function for the Sn second neighbor are out of phase with that for the Cu and Zn functions, as shown explicitly in Fig. 4. Thus, a sum of Cu-Cu and Cu-Sn functions will interfere destructively leading to a low amplitude. This interference makes it difficult to analyze the second-neighbor data without detailed fits.

The EXAFS data also show that both samples have a significant amount of disorder for the second neighbors and beyond. Although the first peak has a large amplitude, the second peak is small compared to theoretical EXAFS functions for undistorted CZTS or EXAFS data for pure ZnS [5,24].

IV. DATA ANALYSIS

A. General fitting and constraints

The kesterite structure, shown in Fig. 1, has a lower formation energy than the stannite structure and thus is the more stable structure [32]. A comparison of kesterite and stannite bond lengths, as measured by diffraction [33], is shown in Table III. The bond lengths of the two structures are within about 0.01 Å of each other, which is indistinguishable to EXAFS. Although all of the metal-metal distances are the same within ±0.01 Å for the kesterite structure, the first Sn—S bond is significantly longer (0.08 Å) than either Zn-S or Cu-S, while the second Sn-S is slightly shorter (−0.03 Å) than the corresponding second Cu-S or Zn-S distances. This indicates some *M-S-M* bond bending within the kesterite structure.

Using the space group parameters for kesterite Cu_2ZnSnS_4 ($I\bar{4}$ space group, $a = 5.427$ Å and $c = 10.848$ Å) [33], theoretical EXAFS functions are calculated for each pair of atoms (metal-S, metal-Cu/Zn, metal-Sn, and the longer metal-S) using the program FEFF8.5 [31]. The first shell of neighbors around the metal atoms in Cu_2ZnSnS_4 contains four S atoms at distances of 2.3–2.4 Å (see Fig. 1 and Table III). The second shell of neighbors around the metal atoms contains the first metal neighbors at a distance of approximately 3.8 Å; the longer metal-S bond (about 4.5 Å) is included to improve the fit results. These bond lengths, as measured by diffraction [33], are shown in Table III. The inclusion of a

TABLE III. The first three columns show diffraction results for the bond lengths and number of neighbors (N) of kesterite and stannite Cu_2ZnSnS_4, generated from Hall *et al.* [33] using ATOMS [34]. The number of neighbors for these first four pairs is identical in the two structures. The final six columns show the Cu K, Zn K, and Sn K fit results for Cu_2ZnSnS_4 at 50 K for sample 1 and 8 K for sample 2, assuming that each metal pair can be modeled with a simple broadened Gaussian pair distribution and that the total number of metal second neighbors is 12. The EXAFS bond lengths (r_E) are in good agreement with diffraction results (r_D) at 300 K [33]. Although the second-neighbor distances are initially constrained by the space group, no significant change in r occurs when this constraint is released. In these fits, except for the Zn K edge of sample 2, the number of Sn neighbors around each metal atom is too large compared to the kesterite structure, and σ^2 for the M-M pairs is large. Errors for the first M-S peak are ±0.01 Å for distance and ±0.0004 Å^2 for σ^2; for the second M-S peak, ±0.02 Å for the distance and ±0.001 Å^2 for σ^2. Errors for Sn- M pairs are ±0.02 Å for distance and ±0.001 Å^2 for σ^2.

			Kesterite	Stannite	No. 1			No. 2		
Edge	Neighbor	N	r_D (Å)	r_D (Å)	r_E (Å)	σ^2 (Å^2)	N	r_E (Å)	σ^2 (Å^2)	N
Cu	S	4	2.328	2.319	2.307	0.005 21	4	2.307	0.004 76	4
	(Cu/Zn)	8	3.837	3.828, 3.853	3.846	0.0091	4.0	3.857	0.009 22	5.5
	Sn	4	3.837	3.828	3.839	0.0184	8.0	3.850	0.0159	6.5
	*S*2	12	4.517	4.520	4.502	0.0143	12	4.501	0.0132	12
Zn	S	4	2.335	2.349	2.335	0.0054	4	2.337	0.0059	4
	(Cu/Zn)	8	3.837	3.828	3.839	0.0137	6.0	3.838	0.0082	8.2
	Sn	4	3.836	3.853	3.839	0.0137	6.0	3.842	0.0085	3.8
	*S*2	12	4.501	4.510	4.470	0.0128	12	4.493	0.0099	12
Sn	S	4	2.409	2.412	2.417	0.003 72	4	2.407	0.003 58	4
	(Cu/Zn)	12	3.837	3.828, 3.853	3.820	0.0161	9.1	3.824	0.0123	9.1
	Sn	0			3.955	0.0113	2.9	3.921	0.0111	2.9
	S2	12	4.475	4.477	4.472	0.0155	12	4.464	0.0116	12

weak multiscattering peak slightly improves the fits above 4.5 Å but has no significant effect in the 3- to 4-Å range. Including this small contribution, there are five peaks in the fits.

The data are then fit in r space to a sum of these EXAFS functions; in principle, there are three parameters per atom pair—amplitude, position (r), and width σ, of the pair distribution function. σ^2 models thermal and static disorder, which lead to a reduction in peak amplitudes. Constraints must also be included, as otherwise there would be too many free parameters, as is discussed by Stern [35].

Since the amplitude for a given pair is given by $NS_\circ^2$, where $S_\circ^2$ is an amplitude reduction factor from multiscattering, $S_\circ^2$ needs to be measured separately. We determine it using the individual sulfides (CuS, ZnS, SnS_2) and use those values for each metal cation (0.85 for Cu, 0.95 for Zn, and 1.00 for Sn).

The Cu K-, Zn K-, and Sn K-edge data for Cu_2ZnSnS_4 (see Fig. 3) are fit using a k range of 3.5–11.5 $Å^{-1}$ for Cu and Zn, and 3.5–12.5 and 3.5–15.5 $Å^{-1}$ for Sn samples 1 and 2, respectively. Fits are performed over r ranges of 1.6–4.8 Å for all edges.

In the fits, the amplitudes and relative pair distances are initially constrained to be consistent with the known kesterite crystal structure as follows. The ratios of the amplitudes for each atom pair are constrained to the ratio of the coordination numbers N—i.e., 4 S first neighbors, 12 metal second neighbors, and 12 further S neighbors. There are two metal-metal peaks: one for the Cu and Zn neighbors, and the other for the Sn neighbors. The number of each type of metal neighbor is started at the values given by diffraction (see Table III), and the ratio of $(Cu/Zn):Sn$ neighbors is then allowed to vary. This ratio of second neighbors is the only amplitude parameter that is varied. For the pair distances, we initially fix the distance ratios to be that of the kesterite structure, but we allow an overall expansion or contraction—seven parameters are varied (one amplitude, one r, and five σ's); 11 degrees of freedom remain for Cu and Zn using Stern's criteria [35]. No significant change in the pair distances occurs when this constraint on distance ratios is released—11 parameters are varied [five r's, five σ's, and the amplitude ratio for $Sn/(Cu/Zn)$ for second neighbors]; about 7 degrees of freedom remain for Cu and Zn, and 9 and 14 for the two samples at the Sn edge.

B. Results

In the initial fits described above, the pair distances agree with diffraction results for kesterite CZTS, as shown in Table III. The first-neighbor distances are especially close: the difference is ≤ 0.01 Å for Zn-S and Sn-S. The largest variation compared to bonds in the kesterite structure is observed for Cu-S, which contracts by about 0.02 Å. CuS and Cu_2S both have a significantly shorter average Cu—S bond length. The slightly shortened bond length in the nanoparticle samples is much closer to that of bulk CZTS. The consistency of the bond lengths affirms that the nanoparticles are within the desired zinc-blende-like structure. The largest deviation, however, is for the Sn-Sn peak in Sn K-edge data; this pair is not present in the kesterite structure and requires some Sn on either a Cu or Zn site. Surprisingly, this distance is significantly longer than expected—by about 0.1 Å.

The second shell of neighbors also has surprising results for these fits using five peaks. The fit to the Cu-edge data does not have the theoretical four Sn neighbors and eight Cu/Zn neighbors of the kesterite structure. Instead, the second-neighbor peak appears to have significantly more Sn neighbors than expected; see Tables III and II. Because the Cu-Sn function is out of phase with that for Cu-Cu (see Fig. 4), there would be increased destructive interference with a larger Cu-Sn peak, which might partially explain the low amplitude for the second peak. However, there is no distribution of Cu, Zn, and Sn on the four kesterite sites that yields significantly more Sn neighbors than Cu/Zn neighbors around Cu.

The excess number of Sn neighbors is also observed in the Zn fits for sample 1; Table III shows there are approximately 6.0 Sn neighbors, significantly more than for the kesterite structure, and more than the calculated number in Table II: 4.4. By contrast, the number of neighbors around Zn in the five-peak fit for sample 2 agrees very well with Table II.

Finally, five-peak fits are also performed on the Sn K-edge data. The Sn—S bond length (about 2.41 Å) is very close to that for the kesterite structure but is significantly different from most other similar compounds; the Sn-Cu/Zn distance is also within ± 0.02 Å of the value for the kesterite structure. These results indicate that Sn is in a kesteritelike lattice. Based on this structure, Sn atoms should not have any Sn second neighbors; however, the fit of the Sn-edge data shows there are approximately 2.9 Sn second neighbors present—slightly higher, even, than the estimates in Table II. Surprisingly, the number of Sn neighbors is roughly the same in both samples. To have Sn-Sn pairs, some antisite Sn must be on the Cu or Zn sites; the excess Sn stoichiometry for sample 1 explains much of the Sn-Sn amplitude. However, sample 2 has nearly the stoichiometric amount of Sn (1.06) and, if only 0.06 Sn were on either a Cu or Zn site, the resulting Sn-Sn peak would be very small. The significant Sn-Sn peak observed for this sample supports the assumptions made in Table II, namely, that excess Zn does not occupy Cu site but goes onto Sn sites, with some Sn moving onto Cu sites. An important feature of the Sn fits is that the distance for the Sn-Sn peak is much longer than any other metal-metal pair distance.

Further fits are performed to test whether the excess Sn could be reduced by adding extra Cu/Zn neighbors at a longer distance. The fits contains the two metal-metal peaks

(Cu-Cu/Zn and Cu-Sn), as before, with the addition of a second Cu-Cu/Zn bond. The extra peak does improve the fit slightly and reduces the number of Sn neighbors a bit—but setting the number of Sn neighbors below 5 (see Table II) makes the fit poor, particularly between 4 and 4.8 Å. Similar results are obtained for sample 1 at the Zn edge.

The possibility of a longer Cu/Zn bond is also tested for the Sn-edge data. The fits contained two Cu/Zn peaks, with one peak initially at a larger distance from the core atom, Sn. The data do not fit this scenario; the long Cu/Zn peak has a huge σ^2 value of 0.159 $Å^{-2}$ and no longer contributes to the EXAFS plot.

It is surprising that the peak at 3.5 Å is so small in the Cu-edge data and in the Zn-edge data for sample 1, as simulations are similar to but somewhat larger than the peak at 3.5 Å in the Zn-edge data for sample 2. In part, the sum of the Cu-Cu/Zn and Cu-Sn peaks near 3.5 Å is relatively small because these two functions are out of phase (see Fig. 4); however, to get the very small amplitude observed requires a very large Cu-Sn peak to cancel the Cu-Cu/Zn peak. Such a large Cu-Sn peak is nonphysical; however, the observed long Sn-Sn distance suggests an alternative possibility. This Sn-Sn distance arises only when there are antisite Sn defects on Cu or Zn sites. Since the first-neighbor Sn—S bond length is very close to that for the kesterite structure, 2.41–2.42 Å, but significantly longer (0.08 Å) than the Cu-S or Zn-S distances, antisite defects will produce displacements of Cu or Zn atoms. Additionally, because the long Sn-Sn second-neighbor distance is about 0.1 Å longer than Cu-Sn or Zn-Sn, there may also be significant changes in the Sn—S—Sn bond angle; increased and decreased bond angles will produce longer and shorter metal-metal pair distances.

One can model such distortions using a Cu-Cu/Zn (or Zn-Cu/Zn) pair distribution that is more complex than a simple Gaussian function. Conceptually, one could add peaks with shorter and longer distances (three peaks in total), but that would introduce four to six additional parameters, depending on the constraints. Alternatively, one could use two Gaussians with quite different widths but the same r's to then have only two additional parameters (one extra σ and an amplitude ratio are needed).

Fits are carried out for these two more-complex Cu-Cu/Zn (and Zn-Cu/Zn for sample 1) distributions; the three-peak model fits best but is only slightly better than the two-peak model with broad and narrow distribution widths. In addition, the ratio of neighbors for these two peaks is almost 1, and setting the amplitudes equal in further fits has very little effect on the quality of the fit. We therefore report the latter, as it requires only one additional parameter σ; those fits are shown in Fig. 5 for the Cu edge and in Fig. 6 for sample 1 at the Zn edge. The fit for sample 2 (the Zn edge) in Fig. 6 uses the five-peak fit described earlier. Likewise, the fits for the Sn edge in Fig. 7 also use the simpler five-peak fit.

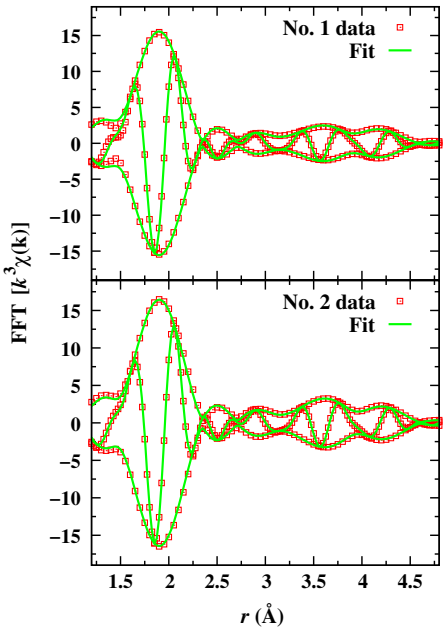

FIG. 5. Fit of the Cu K-edge data using a sum of theoretical functions for kesterite Cu_2ZnSnS_4. The fit range is 1.6–4.8 Å for samples 1 and 2, and the FT range is 3.5–11.5 $Å^{-1}$. These fits use the two-peak model for the Cu-Cu/Zn distribution, as discussed in the text.

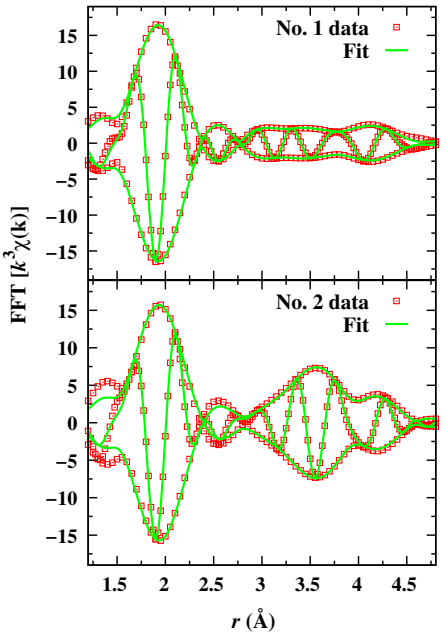

FIG. 6. Fit of the Zn K-edge data for samples 1 and 2 using a sum of theoretical functions for kesterite Cu_2ZnSnS_4. The fit range is 1.6–4.8 Å for both samples, and the FT range is 3.5–11.5 $Å^{-1}$. For sample 1, the Zn-Cu/Zn peak is modeled using two peaks, one narrow and the other broad.

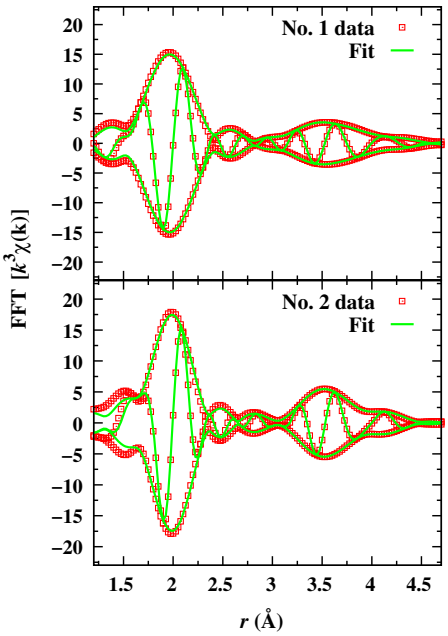

FIG. 7. Fit of the Sn K-edge data for samples 1 and 2 using a sum of theoretical functions for kesterite Cu_2ZnSnS_4. The fit range is 1.6–4.8 Å for both samples, and the FT range is 3.5–12.5 $Å^{-1}$ and 3.5–15.5 $Å^{-1}$ for samples 1 and 2, respectively.

The results from the fits using two Cu-Cu/Zn (or Zn-Cu/Zn) peaks are given in Table IV. Although the number of Sn neighbors for the Cu-edge data is slightly larger than the estimates in Table II, these are reasonable values considering the fact that the disorder is likely more complex. The non-Gaussian disorder for the Cu-Cu/Zn pair distribution, together with the 180° phase shift between Cu-Cu/Zn and Cu-Sn, provides a simple explanation as to why the net peak at 3.5 Å is so small.

For sample 2, there is excess Zn, and some Zn is assumed to move to the Sn sites—see Table II. However, there is then no Sn on the Zn sites. Consequently, the distortions around Zn may be smaller. In fact, the amplitude for Zn-Zn/Cu is more than a factor of 2 larger (at 3.6 Å) than for sample 1. This unusual difference is now easily explained by much less disorder around the Zn atoms because there are no antisite Sn atoms on Zn sites.

The important point in using the two-peak (or three-peak) model is that it allows for a broader distribution of pair distances, with some distances longer or shorter by roughly the lengthening of the Sn-Sn peak; the Sn-Sn peak can occur only when Sn antisite atoms occupy Cu or Zn sites.

V. DISCUSSION

All three edges (Zn, Cu, and Sn K) indicate an excess of Sn second neighbors. This result is consistent with Sn substituting at Cu or Zn sites to form antisite defects in the kesterite structure. Since Cu and Zn are indistinguishable, as mentioned before, the presence of Sn second neighbors provides a strong constraint on the distribution of the metal atoms, particularly around the Sn site. The shortest Sn-Sn distance is significantly longer than other metal-metal distances, which, in turn, suggests that the Sn antisite defects may introduce significant disorder around Cu and Zn, and may lead to split Cu-Cu/Zn or Zn-Zn/Cu peaks, as discussed in the two-peak model above (see Table IV). However, can one exclude the possibility that other impurity phases lead to the number of neighbors and distances observed in Table III instead of using the two-peak model?

First, the M-S bond lengths are all close to that expected for the kesterite structure, which excludes significant fractions of CuS or Cu_2S (Cu—S bonds too short) and SnS or SnS_2 (Sn—S bonds too long), as noted earlier. The M-S peaks are also quite sharp, with values of $\sigma \sim 0.07$ Å ($\sigma^2 \sim 0.005$ $Å^2$). Since part of this width arises from zero-point motion, there is very little variation in the M-S bond lengths. This small width is consistent with the kesterite structure, for which there is one M-S bond length for a given M atom, although bond lengths for different M atoms vary—from 2.31 Å for Cu-S to 2.41 Å for Sn-S. These sharp distributions discriminate against many other compounds, such as $Cu_4Sn_4S_{16}$ and Cu_4SnS_4, which have a broad distribution of Cu-S distances; significant fractions of such compounds would lead to a small Cu-S peak.

TABLE IV. Results for the fits using two Cu-Cu/Zn or Zn-Cu/Zn peaks for the Cu and Zn edges. N_K gives the number of neighbors in the kesterite structure. For the Zn-edge data of sample 2, two Zn-Cu/Zn peaks are not needed; the values with a single peak for Zn-Cu/Zn are included for comparison. Errors are estimated from a range of fits using different starting assumptions; distances have little variation but there are much larger variations for N and σ^2.

			No. 1			No. 2		
Edge	Neighbor	N_K	r_E (Å)	σ^2 ($Å^2$)	N_E	r_E (Å)	σ^2 ($Å^2$)	N_E
Cu	(Cu/Zn)-a	8	3.86(2)	0.0024(5)	3.4(4)	3.85(2)	0.0025(5)	3.4(4)
	(Cu/Zn)-b		3.86(2)	0.034(2)	3.4(4)	3.85(2)	0.017(1)	3.4(4)
	Sn	4	3.81(2)	0.0085(5)	5.2(4)	3.82(2)	0.0091(5)	5.2(4)
Zn	(Cu/Zn)-a	8	3.85(2)	0.0072(5)	3.3(4)	3.84(2)	0.0082(5)	8.2(4)
	(Cu/Zn)-b		3.85(2)	0.014(1)	3.3(4)			
	Sn	4	3.85(2)	0.0126(5)	5.4(5)	3.84(2)	0.0085(5)	3.8(4)

For compounds such as Cu_2SnS_3, there are very nearly twice as many Cu neighbors as Sn neighbors around Cu (as a result of Cu and Sn sharing two sites in the structure), while, for the perfect kesterite structure, there are exactly twice as many Cu/Zn neighbors as Sn around Cu; thus, a significant fraction of this compound could not lead to a smaller number of Cu-Cu/Zn pairs than Cu-Sn pairs. In addition, the Sn—S bond in Cu_2SnS_3 (2.36 Å) is shorter than the Sn-S distance observed in CZTS (2.41 Å), while the Sn-Sn distance in Cu_2SnS_3 (3.83 Å) is much shorter that the Sn-Sn distance observed for CZTS (3.92–3.95 Å). Thus, a significant fraction of ZnS plus Cu_2SnS_3 would not have the distances and amplitudes observed.

$Cu_2Sn_4S_9$, on the other hand, has no Cu or Sn neighbors at distances below 4.3 Å for the Cu site, but six Sn neighbors (and no Cu below 4.3 Å) around the Sn site. These properties are not consistent with the observed distances for Cu-Cu or Cu-Sn near 3.8 Å, or the large number of Cu neighbors around Sn (Table III). We conclude that the best description of the data is a kesterite structure with antisite defects present to accommodate the off stoichiometry. When antisite Sn defects are present, they introduce larger distortions, and broadened pair distribution functions (the two-peak model) for Cu-Cu/Zn or Zn-Cu/Zn pairs are needed. Small fractions of other phases cannot be entirely excluded but are estimated to be, at most, 5%.

A few other papers used EXAFS to examine CZTS materials, with some differing results. Hartman *et al.* [13] detected the presence of ZnS in CZTS thin films by looking at the Zn edge of the data. Their results used EXAFS only for the Zn edge and would be strengthened by data for the other edges. Siah *et al.* [12] looked at the metal and S *K* edges in their EXAFS analysis of the effect of excess Zn, presumably at 300 K. In contrast to Hartman *et al.* [13], their study found that excess Zn is actually incorporated into the CZTS structure via antisite defects and is assumed to be uniformly distributed between the Cu and Sn sites, instead of forming ZnS. This finding partially agrees with our results, which suggest similar antisite defects, but our results for a sample with significant excess Zn suggest that the excess goes more onto Sn sites. This result agrees with earlier work that showed that Cu_2S and ZnS are nearly immiscible [5]. No analysis of the second-neighbor (*M*-*M*) peaks is provided in this paper, and the *M*-S bond lengths have much larger deviations from the kesterite structure (up to 0.07 Å) than in the results reported here.

A third paper reporting EXAFS of CZTS (Bacewicz *et al.* [14]) examined all three metal cation edges in powder samples of CZTS. Their second-neighbor distances agree quite well with our results, although their powders are close to stoichiometric. They proposed that Sn is primarily on its native site but admitted some may be on Cu and Zn defect sites.

Data *et al.* [36] also carried out EXAFS measurements on nanoparticles, presumably at 300 K, and they found considerable disorder for the further neighbor shells. Their metal-S distances agree with our results within 0.01 Å, but they provided no analysis for the further neighbors. Espinosa-Faller *et al.* [16] also agree with our results for the first-neighbor metal-S pairs—to within 0.01 Å. However, the second-neighbor results of our study cannot be directly compared with Espinosa-Faller *et al.* [16] because their analysis described a different number of second neighbors than the kesterite structure. The authors described the theoretical crystal structure for each of the metal cations as having only eight metal second neighbors instead of the 12 given by the structure [14,33]. In Table 2 of their paper [16], Cu was listed as only having four Cu/Zn neighbors, when it should have eight. Espinosa-Faller *et al.* also described Zn as having four Zn second neighbors, even though the kesterite structure contains no Zn second neighbors and eight Cu second neighbors. Similarly, Sn was described by them as having eight Cu/Zn neighbors instead of the expected 12. Finally, their table listed eight neighbors for the second metal-S peak rather than 12 neighbors. The differences in the number of neighbors directly influences the σ^2 values, so these disagreements obstruct comparisons.

Even with the discrepancies for the further neighbors, we agree with the Espinosa-Faller result of site-antisite cation exchange within the crystal structure. The antisite substitution is further supported in that we see no evidence for any interstitial sites in our EXAFS results. Although Espinosa-Faller *et al.* included a few interstitial S sites in their fits of the EXAFS data, the other techniques they used found that interstitial sites played a negligible role. The addition of interstitial S is not required in our EXAFS analysis.

Very recently, Colina-Ruiz *et al.* [17] reported EXAFS at 80 K on highly nonstoichiometric CZTS films with Cu/Zn ratios as low as 1.03 (instead of approximately 2) and Cu/(Zn + Sn) ratios down to 0.64. Thus, some of their films were more nonstoichiometric than the materials considered here. Full details of their fits were not given, but it appears they did not include the possibility of antisite defects in their fits of second neighbors and fixed the amplitudes to that for the kesterite structure. In particular, for the Sn *K* edge, they did not include any Sn-Sn peaks and assumed the Sn-Cu/Zn peak had only eight neighbors. Thus, comparisons to their work for the second-neighbor peaks are not straightforward, as they provide no information about possible antisite defects. However, their *M*-S bond lengths do agree with ours for the samples closest to our compositions. Finally, the bond lengths they tabulated for the kesterite structure do not agree well with the diffraction results of Hall *et al.* [33]; specifically, they listed the *M*-S bond lengths as all being equal (2.35 Å), while Hall *et al.* gave a short bond length for Cu-S (2.328 Å) and a long bond length for Sn-S (2.409 Å).

Nanoparticle films were studied by Turnbull *et al.* [37] using several techniques, including EXAFS. Their sample 1 has a similar composition to our sample 2, but none of the others are comparable to our sample 1, which has a high Sn and a low Cu content. They reported EXAFS results for the first two shells, S and metal neighbors. Unfortunately, the data they showed for the Cu and Zn *K* edges have a very low amplitude for the second neighbors over the range 3–4.8 Å, in contrast to our data and the results of Bacewicz *et al.* [14], and also Data *et al.* [36]. Thus, it is not clear how they obtained detailed fits of the Cu-metal and Zn-metal peaks. Furthermore, most of their reported Cu-metal and Zn-metal distances differ significantly from the kesterite structure; for example, the Cu-Cu distances vary from 3.55 to 3.83 Å, while the Zn-Cu distances vary from 3.67 to 3.91 Å. Such large differences are not found in crystalline materials. In addition, the tabulated distances for the kesterite structure have errors, as there are no Zn-Zn or Sn-Sn second neighbors in a pure kesterite crystal. They also did not discuss the coordination numbers for the second neighbors, which is crucial for probing the effects of nonstoichiometry. Consequently, it is not possible to make a comparison with their results.

Lastly, several groups [12,17–19] have used the S *K*-edge XANES to look at possible impurity phases in nonstoichiometric material. Colina-Ruiz *et al.* [17] used a linear combination of files for CZTS, ZnS, and SnS to fit their S *K*-edge XANES, while Just *et al.* [18] used a linear combination of only CZTS and ZnS scans. Siah *et al.* [12] used the height of the S preedge peak to estimate the amount of ZnS. It is not clear how unique these fits are, as there are many more possible compounds that might be present (e.g., SnS_2, Cu_2SnS_3, $Cu_4Sn_4S_{16}$, and Cu_4SnS_4), all of which might contribute at the S *K* edge. Note that most of the samples investigated by Just *et al.* [18] have Zn/Sn ratios much higher than our samples. Siah *et al.* [12] also focused mostly on Zn-rich samples, while Colina-Ruiz *et al.* [17] had a broad range of stoichiometries. They reported significant amounts of ZnS in some samples, but for samples with compositions similar to our materials, the amount of ZnS present was small.

VI. CONCLUSIONS

In this paper, we carry out a detailed EXAFS study of nonstoichiometric, Cu-deficient, nanoparticle CZTS to determine the structure around each metal atom and ascertain whether significant fractions of the sample might be in other crystalline phases. Cu-deficient materials are of interest because several reports have suggested that such materials are better for devices [1,2,4,22]. From the perspective of EXAFS, these fairly large nanoparticles (7 nm) are close to bulk because the surface layer is only a small fraction of the nanoparticle.

The local structure for the two samples agrees well with the kesterite lattice, with antisite defects, particularly Sn on Cu or Zn sites, accommodating the nonstoichiometry. In particular, the closest *M*-S bond lengths agree with this crystal structure within 0.01 Å for Zn and Sn, and 0.02 Å for Cu. Furthermore, the distributions of these bond lengths are very narrow ($\sigma \sim 0.07$ Å); together, these results indicate that most of the metal atoms are in the kesterite structure and not in some other phases that have different *M*-S bond lengths, such as CuS, Cu_2S, SnS, and SnS_2.

In the Sn-edge data, there are a significant number of second-neighbor Sn atoms observed; since there would be no Sn neighbors for stoichiometric CZTS, this indicates that Sn antisite defects are present on Cu or Zn sites. Surprisingly, the Sn-Sn pairs have a significantly larger pair distance than other *M*-*M* pairs, by about 0.1 Å; this means that there are important local distortions around the antisite Sn defects. Such distortions will lead to broadened distributions for the metal-metal second-neighbor pairs. In the initial fits, we model each pair using a single broadened peak (e.g., Cu-Cu/Zn and Cu-Sn for the Cu edge), but we find nonphysical results in that there appear to be more Cu-Sn pairs than Cu-Cu/Zn pairs around Cu. However, broadening the Cu-*M* further using a two-peak distribution with different widths (or a split peak distribution) models the environment around Cu in both samples and around Zn in sample 1 very well. The distortions around Sn are slightly smaller and are reasonably well described simply by a broadened Sn-Cu/Zn peak.

The results are also consistent with the assumptions used for Table II, namely, that most of the excess Zn in sample 2 goes not onto Cu sites but onto Sn sites, forcing some Sn to move to Cu sites, thereby explaining the Sn-Sn peak observed in this sample. This finding is consistent with earlier work that shows CuS (Cu_2S) and ZnS are not compatible [5,25,38]; note that this work does not exclude low concentrations of antisite defects Cu_{Zn} or Zn_{Cu}, which are often present [6].

These results will be important for theorists trying to model off-stoichiometric material for the optimization of properties. Sn antisite defects appear to form readily on Cu or Zn sites in Cu-poor samples, and our results are consistent with excess Zn, preferring Sn site occupation over Cu site occupation.

More generally, EXAFS is shown to be a good tool for studying the local structure of CZTS, which is likely to be more complicated than stoichiometry suggests. Understanding these structural variations may be a key step to improving solar-energy conversion efficiencies.

ACKNOWLEDGMENTS

This work was initially supported under NSF Grant No. DMR1006190. The experiments were performed at SSRL, operated by the U.S. DOE, Office of Basic Energy Sciences under Contract No. DE-AC02-76SF00515.

[1] W. Wang, M. T. Winkler, O. Gunawan, T. K. Todorov, Y. Zhu, and D. B. Mitzi, Device characteristics of CZTSSe thin-film solar cells with 12.6% efficiency, Adv. Energy Mater. **4**, 1301465 (2014).

[2] Q. J. Guo, G. M. Ford, W. C. Yang, B. C. Walker, E. A. Stach, H. W. Hillhouse, and R. Agrawal, Fabrication of 7.2% efficient CZTSSe solar cells using CZTS nanocrystals, J. Am. Chem. Soc. **132**, 17384 (2010).

[3] H. Katagiri, K. Jimbo, W. S. Maw, K. Oishi, M. Yamazaki, H. Araki, and A. Takeuchi, Development of CZTS-based thin film solar cells, Thin Solid Films **517**, 2455 (2009).

[4] S. Siebentritt and S. Schorr, Kesterites: A challenging material for solar cells, Prog. Photovoltaics **20**, 512 (2012).

[5] A. Short, L. Jewell, A. Bielecki, T. Keiber, F. Bridges, S. A. Carter, and G. Alers, Structure in multilayer films of zinc sulfide and copper sulfide via atomic layer deposition, J. Vac. Sci. Technol. A **32**, 01A125 (2014).

[6] S. Chen, J.-H. Yang, X. G. Gong, A. Walsh, and S.-H. Wei, Intrinsic point defects and complexes in the quaternary kesterite semiconductor Cu_2ZnSnS_4, Phys. Rev. B **81**, 245204 (2010).

[7] C. Malerba, F. Biccari, C. L. Azanza Ricardo, M. Valentini, R. Chierchia, M. Müller, A. Santoni, E. Esposito, P. Mangiapane, P. Scardi, and A. Mittiga, CZTS stoichiometry effects on the band gap energy, J. Alloys Compd. **582**, 528 (2014).

[8] D. B. Mitzi, O. Gunawan, T. K. Todorov, and D. A. R. Barkhouse, Prospects and performance limitations for CuZnSnSSe photovoltaic technology, Phil. Trans. R. Soc. A **371**, 20110432 (2013).

[9] S. Schorr, The crystal structure of kesterite type compounds: A neutron and x-ray diffraction study, Sol. Energy Mater. Sol. Cells **95**, 1482 (2011).

[10] S. Schorr, H.-J. Hoebler, and M. Tovar, A neutron diffraction study of the stannite-kesterite solid solution series, Eur. J. Mineral. **19**, 65 (2007).

[11] R. Nakamura, K. Tanaka, H. Uchiki, T. Washio, and H. Katagiri, Cu_2ZnSnS_4 thin film deposited by sputtering with Cu_2ZnSnS_4 compound target, Jpn. J. Appl. Phys. **53**, 02BC10 (2014).

[12] S. C. Siah, R. Jaramillo, R. Chakraborty, P. T. Erslev, C.-J. Sun, T.-C. Weng, M. F. Toney, G. Teeter, and T. Buonassisi, X-ray absorption spectroscopy study of structure and stability of disordered $(Cu_2SnS_3)_{1-x}(ZnS)_x$ alloys, IEEE J. Photovoltaics **5**, 372 (2015).

[13] K. Hartman, B. K. Newman, J. L. Johnson, H. Dui, P. A. Fernandes, V. Chawla, T. Bolin, B. M. Clemens, A. F. da Cunha, G. Teeter, M. A. Scarpulla, and T. Buonassissi, Detection of ZnS Phases in CZTS Thin-Films by EXAFS, in *Proceedings of the 37th IEEE Photovoltaic Specialists Conference (PVSC), Seattle, 2011* (IEEE, New York, 2011), p. 002506.

[14] R. Bacewicz, J. Antonowicz, S. Posiadło, and S. Schorr, Local structure in Cu_2ZnSnS_4 studied by the XAFS method, Solid State Commun. **177**, 54 (2014).

[15] W. Zalewski, R. Bacewicz, J. Antonowicz, A. Pietnoczka, T. Evstigneeva, and S. Schorr, XAFS study of kesterite, kuramite, and stannite type alloys, J. Alloys Compd. **492**, 35 (2010).

[16] F. Espinosa-Faller, D. R. Conradson, S. C. Riha, M. B. Martucci, S. J. Frederick, S. Vogel, A. L. Prieto, and S. D. Conradson, Neutron diffraction and x-ray absorption fine structure evidence for local lattice distortions and aperiodic antisite substitution in Cu_2ZnSnS_4 nanoparticles, J. Phys. Chem. C **118**, 26292 (2014).

[17] R. Colina-Ruiz, J. M. de Len, J. Lezama-Pacheco, F. Caballero-Briones, M. Acosta-Alejandro, and F. Espinosa-Faller, Local atomic structure and analysis of secondary phases in non-stoichiometric Cu_2ZnSnS_4 using x-ray absorption fine structure spectroscopy, J. Alloys Compd. **714**, 381 (2017).

[18] J. Just, D. Lutzenkirchen-Hecht, R. Frahm, S. Schorr, and T. Unold, Determination of secondary phases in kesterite Cu_2ZnSnS_4 thin films by x-ray absorption near edge structure analysis, Appl. Phys. Lett. **99**, 262105 (2011).

[19] J. Just, C. M. Sutter-Fella, D. Lutzenkirchen-Hecht, R. Frahm, S. Schorr, and T. Unold, Secondary phases and their influence on the composition of the kesterite phase in CZTS and CZTSe thin films, Phys. Chem. Chem. Phys. **18**, 15988 (2016).

[20] S. Jang, B. D. White, I. K. Lum, H. Kim, M. A. Tanatar, W. E. Straszheim, R. Prozorov, T. Keiber, F. Bridges, L. Shu, R. E. Baumbach, M. Janoschek, and M. B. Maple, Resolution of the discrepancy between the variation of the physical properties of $Ce_{1-x}Yb_xCoIn_5$ single crystals and thin films with Yb composition, Philos. Mag. **94**, 4219 (2014).

[21] F. Bridges, C. MacKeen, and L. Kovács, No difference in local structure about a Zn dopant for congruent and stoichiometric $LiNbO_3$, Phys. Rev. B **94**, 014101 (2016).

[22] H. Katagiri and K. Jimbo, Development of rare metal-free CZTS-based thin film solar cells, in *Proceedings of the 37th IEEE Photovoltaic Specialists Conference (PVSC), Seattle, 2011* (IEEE, New York, 2011), p. 003516.

[23] Q. J. Guo, H. W. Hillhouse, and R. Agrawal, Synthesis of Cu_2ZnSnS_4 nanocrystal ink and its use for solar cells, J. Am. Chem. Soc. **131**, 11672 (2009).

[24] C. Corrado, Y. Jiang, F. Oba, M. Kozina, F. Bridges, and J. Z. Zhang, Synthesis, structural, and optical properties of stable ZnS:Cu,Cl nanocrystals, J. Phys. Chem. A **113**, 3830 (2009).

[25] J. Stanley, Y. Jiang, F. Bridges, S. A. Carter, and L. Ruhlen, Degradation and rejuvenation studies of ac electroluminescent ZnS:Cu,Cl phosphors, J. Phys. Condens. Matter **22**, 055301 (2010).

[26] See http://lise.lbl.gov/RSXAP/.

[27] J. A. Victoreen, The calculation of x-ray mass absorption coefficients, J. Appl. Phys. **20**, 1141 (1949).

[28] E. A. Stern and K. Kim, Thickness effect, Phys. Rev. B **23**, 3781 (1981).

[29] S. M. Heald, in *X-Ray Absorption: Principles, Applications, Techniques of EXAFS, SEXAFS, XANES*, edited by D. Koningsberger and R. Prins (John Wiley & Sons, New York, 1988), p. 87.

[30] W. H. McMaster, Lawrence Radiation Laboratory Report No. UCRL-50174, Sect. II, Revision 1, 1969.

[31] A. L. Ankudinov, B. Ravel, J. J. Rehr, and S. D. Conradson, Real space multiple scattering calculation of XANES, Phys. Rev. B **58**, 7565 (1998).

[32] M. Jiang and X. Yan, Cu_2ZnSnS_4 Thin Film Solar Cells: Present Status and Future Prospects, in *Solar Cells—Research and Application Perspectives*, edited by A. Morales-Acevedo (InTech, Rijeka, Croatia, 2013), p. 107.

[33] S. R. Hall, JT. Szymanski, and J. M. Stewart, Kesterite, $Cu_2(Zn, Fe)SnS_4$, and stannite, $Cu_2(Zn, Fe)SnS_4$, structurally similar but distinct minerals, Can. Mineral. **16**, 131 (1978).

[34] B. Ravel, ATOMS: Crystallography for the x-ray absorption spectroscopist, J. Synchrotron Radiat. **8**, 314 (2001).

[35] E. A. Stern, Number of relevant independent points in x-ray-absorption fine-structure spectra, Phys. Rev. B **48**, 9825 (1993).

[36] P. Data, M. Bialoglowski, K. Lyzwa, R. Bacewicz, P. Dluzewski, M. Lapkowski, T. Gregorkiewicz, S. Podsiadlo, and A. P. Monkman, Kesterite inorganic-organic heterojunction for solution processable solar cells, Electrochim. Acta **201**, 78 (2016).

[37] M. J. Turnbull, D. Vaccarello, Y. M. Yiu, T.-K. Sham, and Z. Ding, Identifying barriers to charge-carriers in the bulk and surface regions of Cu_2ZnSnS_4 nanocrystal films by x-ray absorption fine structures (XAFSs), J. Chem. Phys. **145**, 204702 (2016).

[38] E. Lendvay, Formation of Cu_xS and Zn secondary phases in ZnS single crystals, J. Cryst. Growth **59**, 384 (1982).